Phosphorescence and donor-acceptor pair recombination in laboratory-grown diamonds

Jiahui Zhao (赵嘉慧),[1,*] Ben L. Green,[1] Ben G. Breeze,[2] and Mark E. Newton[1,†]
[1]*Department of Physics, University of Warwick, Coventry CV4 7AL, United Kingdom*
[2]*Spectroscopy Research Technology Platform, University of Warwick, Coventry CV4 7AL, United Kingdom*

(Received 2 June 2023; accepted 15 September 2023; published 27 October 2023)

Intense "blue-green" phosphorescence is commonly observed in near-colorless laboratory-grown high-pressure high-temperature diamonds following optical excitation at or above the indirect band gap. We have employed a holistic combination of optically excited time-resolved techniques (in addition to standard spectroscopic characterization techniques) to study the physics of this long-lived phosphorescence and understand luminescence-related charge-transfer processes. It is shown that the properties of the broad "blue-green" luminescence and phosphorescence band can be fully explained by emission from neutral substitutional nitrogen-boron donor-acceptor pairs ($N_S^0 \cdots B_S^0$), once the configurational change between charge states is considered, and both tunneling between defects and thermal ionization of donors and acceptors is considered. Significant concentrations of metastable N_S^- are identified after optical excitation at or above the indirect band gap. N_S^- is much shallower (~0.2 eV) than previously thought and plays a key role in resetting the $N_S^0 \cdots B_S^0$ donor-acceptor pairs.

DOI: 10.1103/PhysRevB.108.165203

I. INTRODUCTION

Diamond is a wide-band-gap material ($E_G = 5.47$ eV; indirect) with large donor (nitrogen: $E_D = 1.7$ eV [1]; phosphorus: $E_D = 0.62$ eV [2]) and acceptor (boron: $E_A = 0.368$ eV [3]) ionization energies. If, during the production of diamond by high-pressure high- temperature (HPHT) synthesis, a sufficient concentration of nitrogen getters [4] is added to the growth capsule, the concentration of substitutional nitrogen (N_S) impurities incorporated into the diamond can be reduced to less than 200 ppb (parts per billion carbon atoms). The resulting diamond samples typically contain similar concentrations of substitutional boron (B_S) impurities. Such diamonds would be classified as type II [5]. Phosphorescence, or delayed luminescence, is commonly observed in such HPHT diamonds after illumination with light of energy equal to or greater than the indirect band gap. The phosphorescence lasts for a few milliseconds up to several hours after the removal of optical excitation [6,7]. Combinations of phosphorescence imaging and other spectroscopic identification techniques are routinely used to distinguish laboratory-grown HPHT diamonds from natural diamonds [8].

A "blue-green" phosphorescence band, with a peak energy of 2.5(1) eV (490–503 nm), is often observed in type II natural, HPHT synthetic, and HPHT treated diamonds [6–15]. There is a lack of research on phosphorescence in chemical vapor deposition (CVD) synthetic diamonds. Almost all phosphorescence in natural, HPHT synthetic, and HPHT treated diamonds detected after band-gap excitation at room temperature contains the "blue-green" component. The "blue-green" phosphorescence is quenched at higher temperatures, and the band position is temperature-independent in a range of 250–400 K [15,16]. The "blue-green" emission band was not seen after excitation with light of wavelengths 365 and 458 nm [6,10].

In previous work, the "blue-green" phosphorescence has been suggested to originate from temperature-dependent ionization of substitutional boron acceptors combined with recombination emission at donor-acceptor pairs (DAPs) [6]. However, questions about the defects involved and the details of the mechanism remain. The incorporation of defects/impurities in HPHT diamond is growth-sector-dependent, and the differences in phosphorescence behavior between growth sectors significantly complicates analysis in multisectored samples. The nature of the donor and the involvement of other defects or luminescence centers needs to be investigated. The temperature dependence of phosphorescence has not been fully investigated: phosphorescence observed at liquid nitrogen temperature cannot be explained by the thermal excitation mechanism proposed in the literature (see Sec. III C 3 below). Furthermore, it is somewhat surprising that low concentrations of impurities/defects in type II HPHT diamonds are sufficient to give rise to the intense phosphorescence that is often observed.

The energy obtained from electromagnetic or ionizing radiation (such as optical excitation, x-rays, or electron irradiation) can be stored in the diamond by trapping charge carriers at defects. After excitation, a fraction of the stored energy can be released as phosphorescence; in other cases, the

*gloria.zhao.1@warwick.ac.uk
†m.e.newton@warwick.ac.uk

energy can be stored in the dark for a long time and is released as thermoluminescence (TL) when heated, via thermally activated detrapping of charge carriers [13,17]. Therefore, TL is a useful technique to investigate the interaction between traps and optically active defects in diamond. The shape, position, and intensity of the TL emission ("glow curve") indicates the depth and the relative concentration of traps [17,18]. "Blue-green" and "red" TL is seen in natural, HPHT synthetic, and boron-doped CVD synthetic diamonds, regardless of type I or type II [11,13,19–24]. The "blue-green" TL band centered at 2.57 eV [19] or 2.6 eV [11] seen after UV illumination could be linked to the "blue-green" phosphorescence band observed by Shao *et al.* [25]. TL emission which peaks at 480 K after UV illumination in a weakly boron-doped type IIb CVD synthetic diamond film has a broad spectral band centered at ∼490 nm, close to the "blue-green" phosphorescence band position [26]. Thus the same defects may play roles as luminescence centers in both phosphorescence and thermoluminescence [11]. Two TL glow peaks corresponding to traps with activation energies of approximately 0.2 and 0.37 eV are commonly observed in type II natural and HPHT synthetic diamonds [11,20–22,27]. The TL glow peak of activation energy of 0.37 eV is widely agreed to be assigned to substitutional boron acceptor. However, the trap identified from the lower activation energy TL peak is uncertain: Walsh considered it as a shallower acceptor [11], while Bourgoin believed its energy level is approximately 0.22 eV below the conduction band [22]. It is notable that this TL glow peak is more intense in diamond samples containing a higher concentration of nitrogen [11].

In this research, time-resolved Fourier-transform infrared (FTIR) absorption and time-resolved electron paramagnetic resonance (EPR) techniques are used to understand the role of B_S and N_S defects in the charge-transfer processes, in order to explain the phosphorescence and thermoluminescence behavior in the HPHT laboratory-grown diamond samples studied. The incorporation efficiency of boron is highly growth-sector-dependent in HPHT laboratory-grown diamonds [28–30]. Higher HPHT crystallization temperature results in increased uncompensated boron concentration in the {111} and {100} growth sector [29]. The rate of uptake boron by various growth sectors of HPHT diamond is {111} > {110} > {100}, {113} [31]. In HPHT diamonds, the preference for nitrogen incorporation is also growth-sector-dependent, and the nitrogen content usually follows {111} > {100} > {113} > {110} [31,32]. Substitutional nitrogen N_S is also known as the C-center or P1 defect in EPR studies.

In principle, at room temperature and below, the Fermi energy of an N- or B-doped diamond is pinned close to the N_S^0 donor or B_S^0 acceptor level, depending on which is present in the higher concentration. Due to the relatively deep donor/acceptor levels, the probability of thermally ionizing the N_S^0 donor is negligible, and only a very small faction (<1%) of the B_S^0 acceptors will be ionized at room temperature. However, in an insulating material like diamond, the calculated position of the Fermi level does not necessarily predict the correct charge state of a defect, and multiple charge states of the same defect can be present at the same time [33]. In this situation, the charge state of a defect is influenced by its proximity to a donor (or acceptor) and the optical excitation/thermal history of the diamond. Thus, N_S^0, N_S^+, B_S^0, and B_S^- are all expected to be present in a diamond containing low concentrations of both B_S and N_S. Furthermore, substitutional nitrogen has been predicted to have an acceptor level (N_S^-) lying approximately 1.1 eV below the minimum of the conduction band [34]. Experimental evidence for N_S^- was provided by ultrafast spectroscopic measurements in which a transient infrared absorption feature at 1349 cm^{-1} was assigned to a local vibrational mode of N_S^- [35].

In previous studies of charge transfer and phosphorescence in near-colorless HPHT grown diamond, the role of N_S^- has not been considered, while in this work the existence of N_S^- is shown to be crucial for the interpretation of the data and is found to be a much shallower donor than previously predicted [34].

TABLE I. The concentrations of B_S^0 and N_S^0 in samples B{001} and C{111} in the "metastable ambient state."

Concentration (ppb)	B{001}	C{111}
$[B_S^0]$ by FTIR	67 ± 10	332 ± 40
$[N_S^0]$ by EPR	145 ± 20	<4

II. EXPERIMENTAL DETAILS

A. Samples

The single-crystal diamond samples GE81-107a-B and GE81-107a-C were grown using the temperature gradient method by General Electric with iron cobalt solvent-catalyst and an aluminum nitrogen getter. From the as-grown sample, a {110} oriented plate (∼0.85 mm thick) was prepared and subsequently cut and polished into separate samples: GE81-107a-B (B{001} henceforth) is dominated by {100} growth sector but also contains some other minor growth sectors, and GE81-107a-C (C{111} henceforth) consists of a {111} growth sector. Both samples were near-colorless but weakly boron-doped and present characteristic "blue-green" fluorescence under band-gap UV excitation, with subsequent long-lived phosphorescence. The average concentration of B_S^0 and N_S^0 in both samples in the "meta-stable ambient state" (e.g., at room temperature after daylight/laboratory illumination for >1 h) was determined by FTIR absorption and EPR spectroscopy (see Table I).

B. Time-resolved FTIR

To study B_S-related charge transfer during phosphorescence decay, an optically excited variable temperature FTIR absorption experiment was set up using a Thermo Fisher Scientific Nicolet iS50R FTIR spectrometer. The diamond sample was cooled or heated to a selected temperature between 273 and 573 K by a variable temperature stage (Linkam THMS600), and a reference spectrum was collected with the sample in the dark. A 224 nm pulsed laser (Photon Systems HEAG70-224SL) operating at 10 Hz was focused on the sample until the B_S^0 absorption reached a steady state under optical excitation (saturation). After saturation was achieved, the optical excitation was removed, and the FTIR

spectrometer triggered to collect spectra every 210 ms by an Arduino. Thus the decay of the 2802 cm^{-1} B_S^0 absorption peak was recorded during the phosphorescence decay [36].

C. Time-resolved EPR

The decay/recovery of the N_S^0 concentration post-optical-excitation was monitored in an optically excited variable temperature EPR experiment utilizing a Bruker E580 spectrometer equipped with an X-band microwave bridge. A Bruker ER4131 VT temperature controller was used to cool or heat the sample to a temperature between 160 and 400 K. After optical excitation to saturation (i.e., no further change in N_S^0 EPR signal) with the 224 nm laser, the EPR spectrometer was triggered to start rapid-passage scans in the dark at a sweep frequency of 10 Hz and a sweep width of 2 mT across the central line of the N_S^0 EPR spectrum. A National Instruments CompactRIO controller combined with NI-9219 and NI-9264 modules was used to control the drive of the field sweep coils (sweep rate up to 200 mT/s), and ensure synchronization with the EPR data acquisition [37].

D. Luminescence

An Edinburgh Instruments FS5 spectrofluorometer was used to measure the excitation dependence of photoluminescence in the diamonds at room temperature over an excitation range of 200–500 nm and an emission range of 200–800 nm.

Cathodoluminescence spectra were recorded by a scanning electron microscope equipped with a Gatan Mono CL system at 80 K and room temperature.

An experimental system was built to study phosphorescence and TL in diamond, which enabled time-resolved bulk spectral and hyperspectral acquisition, when combined with the 224 nm pulsed laser. The sample was mounted in a variable temperature stage (Linkam THMS600) with the working temperature range between 83 and 873 K. Sample emission was detected by either a fiber-coupled spectrometer (ANDOR Shamrock i303) operating between 400 and 1000 nm, or a camera (HAMAMATSU CMOS C11440-36U) sensitive to 300–1100 nm. The hardware components, including the laser, temperature stage, filters, and detectors, were controlled by an Arduino Uno, which enabled ~ms time accuracy in phosphorescence and thermoluminescence experiments. To perform a phosphorescence experiment, the diamond sample was cooled or heated to a selected temperature in the absence of optical excitation and then optically excited to saturation of the initial phosphorescence emission before detection was triggered. When performing a TL experiment, the sample was cooled to 83 K and optically excited to saturation. After the light source was removed, the sample was then heated up to 473 K at a linear rate of 100 K/min after a variable delay time. TL glow was recorded by the camera or spectrometer. The "thermal cleaning" method (Fig. 1) was used to separate overlapping TL glow peaks: after initial optical excitation at 83 K, the sample was heated as in a normal TL experiment, but cooled back down to 83 K just after the maximum intensity of each distinct TL peak was reached. This procedure was repeated until all peaks were detected [17].

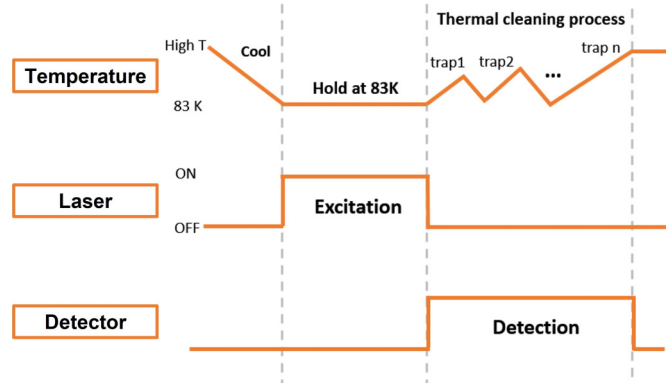

FIG. 1. Schematic of the thermoluminescence (TL) experiment sequence for deconvolving multiple overlapping TL peaks (known as "thermal cleaning" [17]).

III. RESULTS

A. B_S^0 related charge transfer

Above-band-gap UV excitation increased the concentration of uncompensated substitutional boron in both samples, as measured by FTIR. As the sample temperature was increased, the UV illumination had less of an effect on the B_S^0 concentration. Post-excitation decay curves of the 2802 cm^{-1} B_S^0 absorption peak intensity show the decay rate is temperature-dependent (Fig. 2). The data are plotted on a logarithm timescale to emphasize the change in the decay rates. Consistent with literature reports, the B_S^0 2802 cm^{-1} absorption peak decays during phosphorescence [38,39]. At each temperature, the $[B_S^0]$ decay rate in the {111} growth sector is slower than that in the (lower boron concentration) {001} growth sector.

B. N_S^0 related charge transfer

Rapid-passage, post-UV-illumination measurements of the central peak of the N_S^0 EPR spectrum (plotted as an integrated intensity) in sample C{111} [Fig. 3(a)] show that $[N_S^0]$ is increased during the UV-illumination and decays post-illumination in this sample [40]. The lifetime of the N_S^0 concentration decay is temperature-dependent: the higher the temperature, the shorter the lifetime (the lifetime varies by a factor of >5 between 210 and 250 K).

Conversely, the metastable N_S^0 concentration in sample B{001} is reduced by 224 nm laser excitation in the temperature range 270–347 K: the central peak of the N_S^0 EPR spectrum recovers on a timescale of tens of seconds after the removal of UV illumination [Fig. 3(b)]. The recovery rate is strongly temperature-dependent between 270 and 318 K, whereas it only becomes slightly faster as the temperature is increased above 318 K. It should be noted that above 290 K the metastable N_S^0 concentration is strongly temperature-dependent, decreasing as the temperature is increased.

C. Luminescence

1. Photoluminescence

Two-dimensional room-temperature photoluminescence excitation experiments allow us to measure the excitation

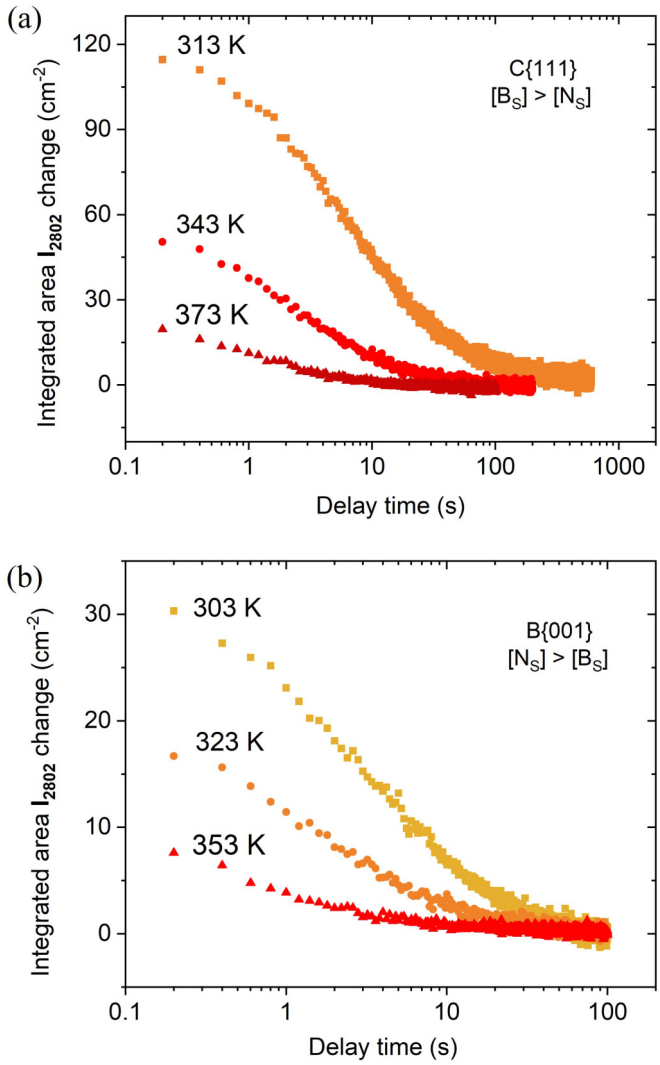

FIG. 2. The integrated area of 2802 cm^{-1} peak recorded post-illumination with a 224 nm laser for (a) sample C{111} where $[B_S] > [N_S]$, and (b) B{001} where $[N_S] > [B_S]$. In both samples, the B_S concentration decreases once optical excitation is removed.

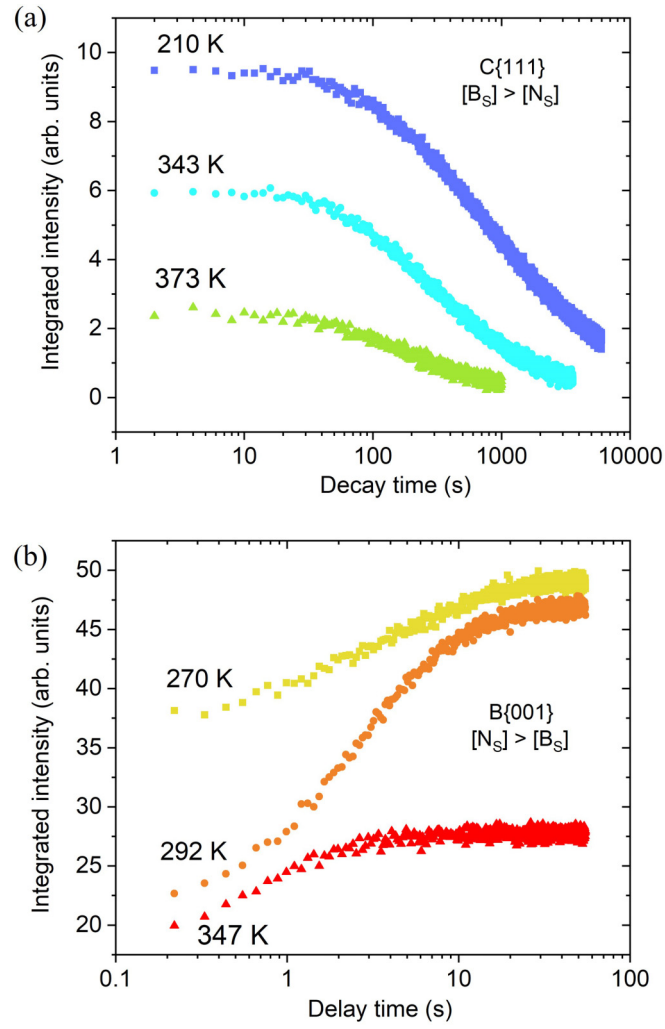

FIG. 3. Time-resolved integrated intensity of the central N_S^0 hyperfine peak following 224 nm illumination, as measured by rapid-passage EPR for sample (a) C{111} where $[B_S] > [N_S]$, and (b) B{001} where $[N_S] > [B_S]$.

dependence of the "blue-green" luminescence band centered at approximately 2.5 eV in the diamond samples studied [Fig. 4(a)]. The center of the band shifts from 490 to 480 nm as the excitation wavelength varies from 200 to 235 nm. The luminescence band is most intense under ~222.5 nm excitation [Fig. 4(b)]. It is clear that in order to excite the "blue-green" emission, an excitation wavelength shorter than ~235 nm is required. Interestingly, this corresponds to the free-exciton emission energy in a diamond. Thus it appears that excitation to produce free electrons and holes is required to observe the "blue-green" emission: radiative relaxation can then occur via reasonably close donor-acceptor pair recombination.

2. Cathodoluminescence

Cathodoluminescence spectra from both growth sectors at 80 K and room temperature show strong emission bands, and the peak intensity shifts to lower energy as the sample temperature is reduced. The CL emission band from sample B{001} is centered at 532 nm (2.33 eV) and 503 nm (2.46 eV) at 80 K and room temperature, respectively (Fig. 5); the CL emission band in sample C{111} is peaked at 535 nm (2.32 eV) and 520 nm (2.28 eV) at 80 K and room temperature, respectively. It is notable that in sample B where $[N_S] > [B_S]$, an extra UV emission band centered at 390 nm (3.2 eV) presents at 80 K, which is not observed in sample C where $[B_S] > [N_S]$.

3. Phosphorescence

Characteristic "blue-green" phosphorescence is observed in both samples post-224 nm excitation between 83 and 473 K. The phosphorescence band in sample C{111} peaks at 2.25 eV (550 nm) in the low-temperature range of 83–173 K, and approximately 2.5 eV (494 nm) at high temperature between 273 and 473 K (Fig. 6). There is no shift in the band peak energies during decay in either of these low (83–173 K) or high (273–473 K) temperature ranges. The 2.5 eV band corresponds to the phosphorescence reported in the literature

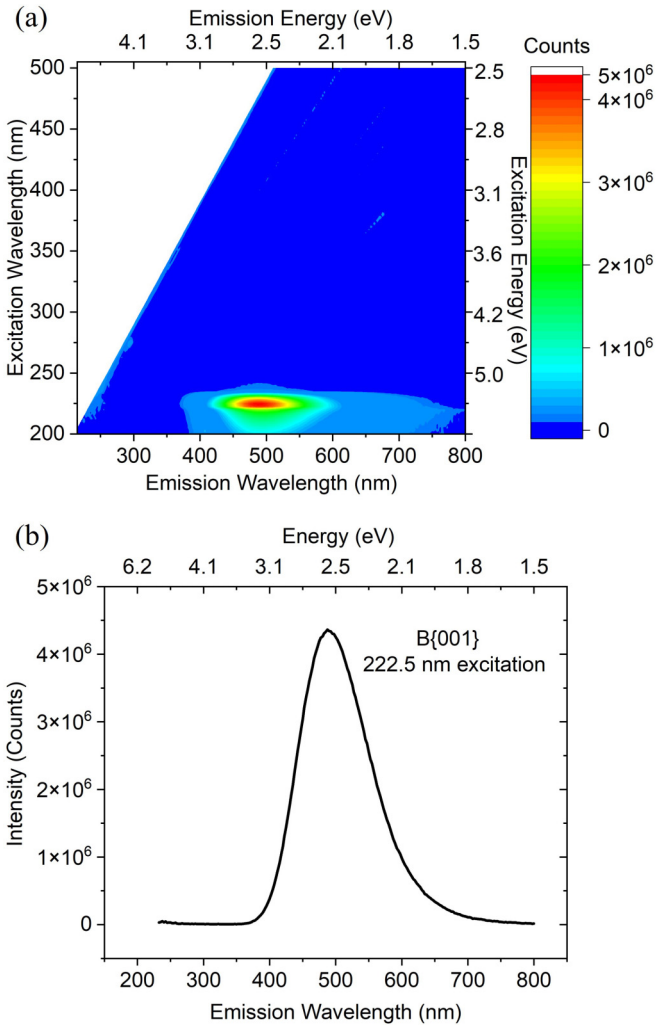

FIG. 4. (a) Photoluminescence excitation spectra of sample B{001} at room temperature under excitation ranging from 200 to 500 nm. (b) Photoluminescence spectrum under 222.5 nm excitation.

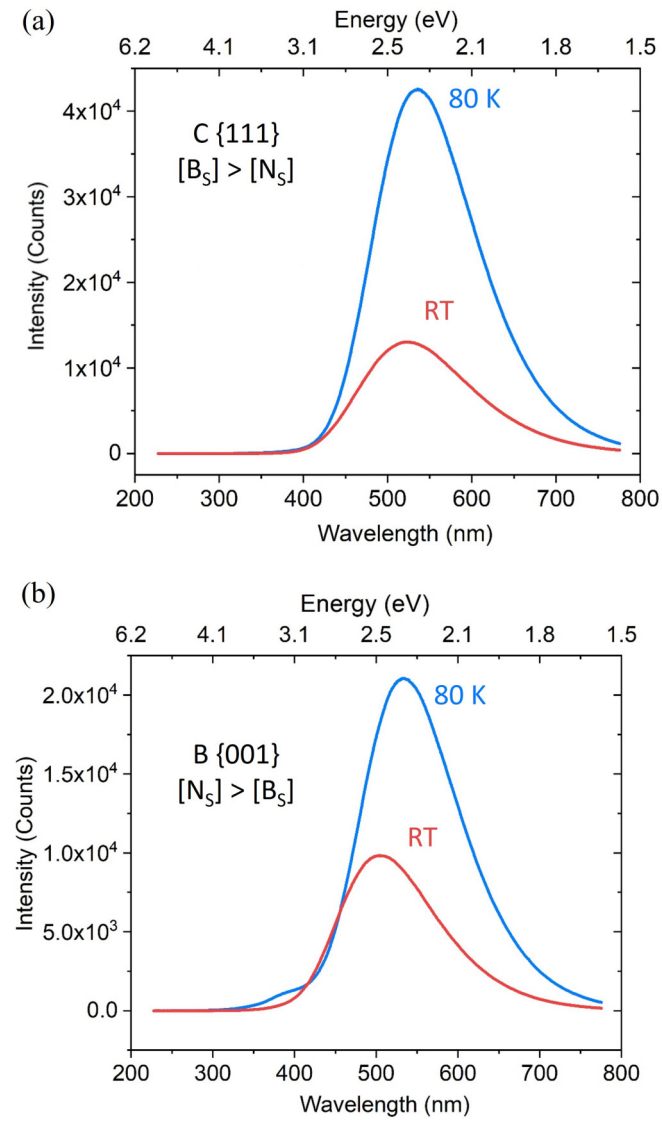

FIG. 5. CL spectra at 80 K and room temperature (RT) in sample (a) C{111} where $[B_S] > [N_S]$, and (b) B{001} where $[N_S] > [B_S]$.

[6,8–11]. In the intermediate temperature range (173–273 K), the emission band position shifts to higher energy significantly during decay, which suggests the mechanisms of phosphorescence switch within this temperature range and the emission consists of at least two components: a phosphorescence band peaked at lower energy which decays faster than a phosphorescence band peaked at higher energy.

The temperature dependence of the emission band position in both samples is similar. At low temperatures (83–173 K), the phosphorescence band is also centered at 2.25 eV (550 nm) in B{001}, same as that in C{111}. At high temperatures above 273 K, the "blue-green" phosphorescence band in B{001} is centered at 484 nm, slightly shorter in wavelength than that of C{111} (494 nm).

In our experiment, phosphorescence intensities are plotted in arbitrary units, but nevertheless a comparison can be made between the relative intensities in both samples since the acquisition parameters are the same for all measurements (Fig. 7). The phosphorescence was more intense in C{111} than that in B{001} at all temperatures studied, but the difference was largest for the measurements in the low- and high-temperature ranges. The phosphorescence decay rate and emission spectrum at low temperatures (83–173 K) in both samples are approximately temperature-independent. At temperatures above 173 K, the phosphorescence lifetime decreased rapidly as the temperature was increased until the decay was too fast to be detected by the experimental setup above 473 K.

A multiple component fitting method (see Appendix A 1) was used to interpret the dominant phosphorescence mechanism at different temperatures. The phosphorescence decay curves at low temperatures (83–173 K) can be satisfactorily fit using two athermal power-law decay components with different parameters, which suggests that the phosphorescence decay in this temperature range originates from athermal tunneling processes. At temperatures above 273 K, the decay can be fitted using two simple exponential curves, suggesting the phosphorescence at high temperature is dominated by thermal activation. Notably, better fitting is achieved by simple exponential functions than hyperbolic functions, which suggests

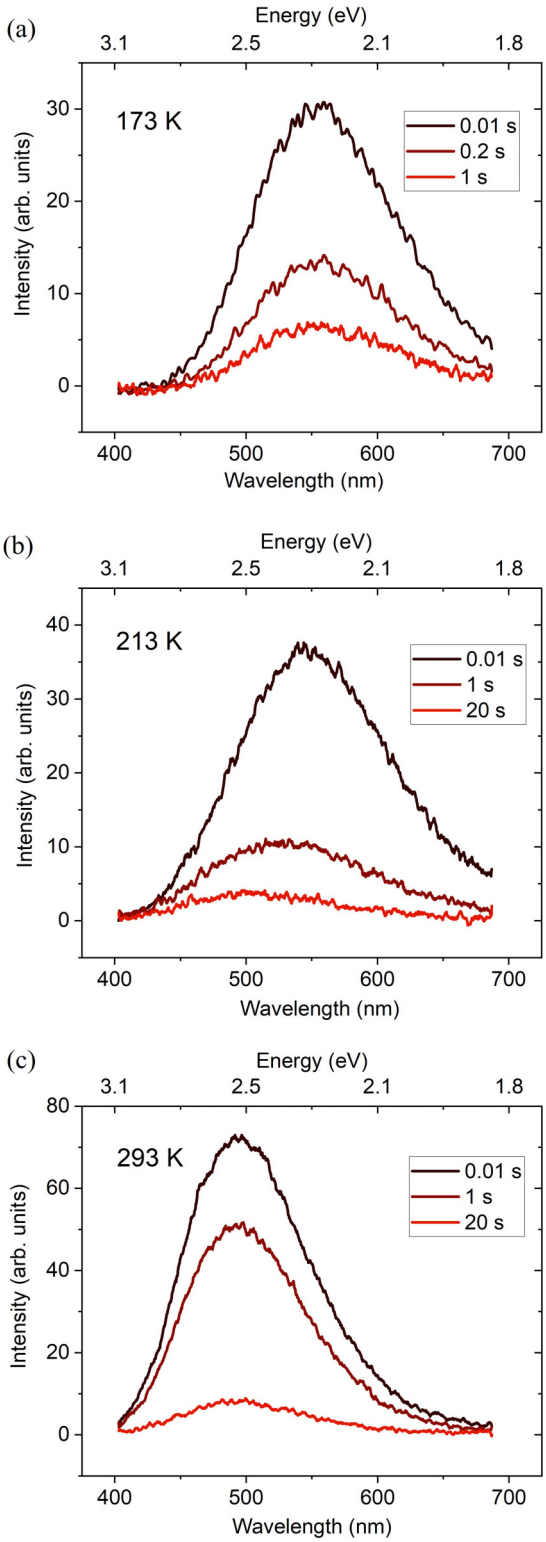

FIG. 6. Phosphorescence spectra (labeled by the delay time between switching off the laser and starting acquisition) of sample C{111} recorded post-224-nm excitation at (a) 173 K, (b) 233 K, and (c) 293 K.

the thermal processes follow first-order kinetics and charge retrapping is negligible. At an intermediate temperature (173–273 K), the phosphorescence decay curve is best-fitted using a combination of athermal power-law decay functions and simple exponential functions, suggesting that both tunneling and thermal activation contributes to phosphorescence at these temperatures.

4. Thermoluminescence

Even at low temperature, following 224 nm excitation there is significant phosphorescence generated: this can interfere with thermoluminescence measurements if the temperature is ramped immediately post-illumination. By delaying the start of the temperature ramp, we ensure the phosphorescence has completely decayed before beginning the thermoluminescence measurement (Fig. 8). As a result, the detected thermoluminescence only arises from the luminescence centers which are located far from the traps, and luminescence that arises from the tunneling process (i.e., near pairs that relax via phosphorescence) was excluded.

The TL intensity in C{111} is stronger than that in B{001}, while the shape and position of the TL glow curves are similar: a single asymmetric TL glow peak was observed from 173 K to approximately 400 K and centered at 273 K. The low-temperature side of the TL peak (173–273 K) corresponds to the "intermediate temperature range" of phosphorescence discussed above. The high-temperature side of the TL peak has a larger half-width than the low-temperature side, which indicates that the TL peak is likely to consist of more than one TL peak overlapping with each other [17].

The solid black line in Fig. 8 represents the TL glow curve recorded under the same conditions but with no delay time between the removal of excitation and the initiating of the temperature ramp. The integrated area of the whole TL glow curve depends on the total number of luminescence centers, regardless of whether they are spatially close to traps or not [41]. At low temperatures, charge tunneling occurs, and phosphorescence originates from donor-acceptor pairs. After this decay, there is still a significant concentration of neutral donors and acceptors that are physically isolated. It is not until the temperature is increased that these donors/acceptors are thermally ionized and release carriers that reset the close DAPs (luminescence centers), so they can emit multiple times and give rise to strong luminescence.

The thermoluminescence spectra (recorded after the phosphorescence has decayed) presents as one featureless broadband centered at 484 nm and 490 nm (∼2.5 eV) for B{001} and C{111}, respectively. There is no shift in TL band position during heating for both samples.

By performing a "TL cleaning" experiment (Fig. 1), two independent TL glow peaks were obtained in both samples. When the temperature of peak intensity for "Peak 1" was reached, the sample was cooled at 50 K min^{-1}, and the thermoluminescence intensity dropped rapidly to zero. The symmetry of "Peak 2" observed during subsequent reheating is typical of second-order kinetics (indicating that retrapping dominates) [17]. Thus if the capture cross-section of the trap and luminescence center is equal, the number of luminescence centers is significantly less than that of traps. As shown in Fig. 9, the spectral positions of maximum thermoluminescence emission in sample C{111} for "Peak 1" and "Peak 2" are both centered at 490 nm, which suggests free carriers thermally released from traps of different depth enable light emission from the same type of luminescence centers.

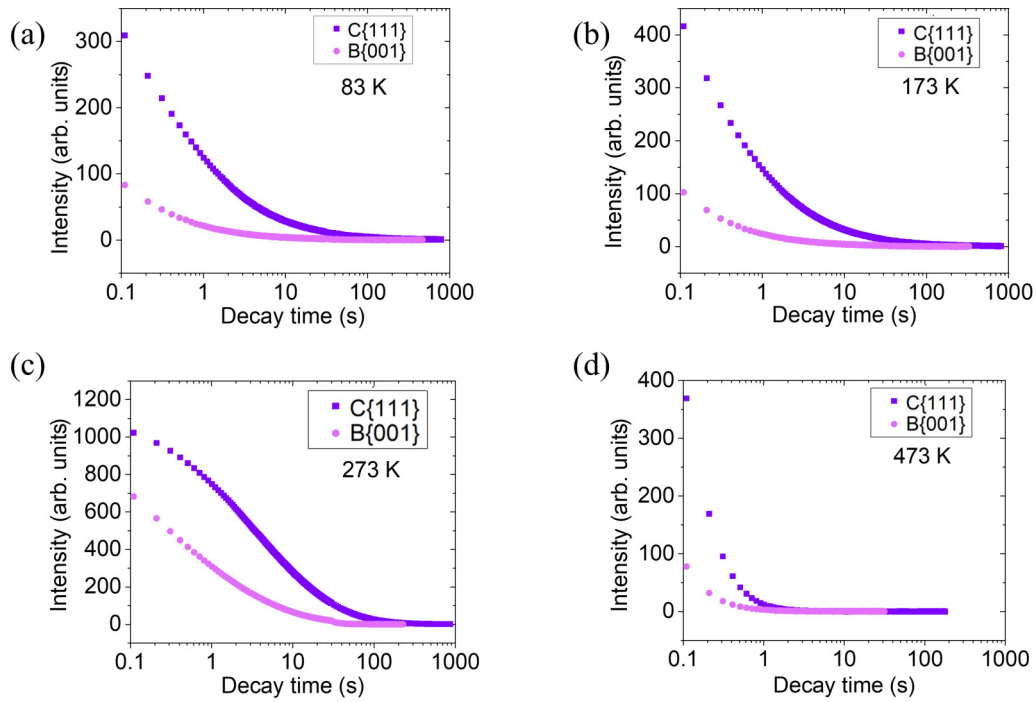

FIG. 7. Phosphorescence intensity decay curves recorded (50 ms acquisition time for each frame) post-224-nm excitation for samples C{111} and B{001} at different temperatures.

IV. DISCUSSION

A. Determination of activation energies

The post-illumination decay/recovery curves shown in Figs. 2, 3, and 7 can be fitted using different methods, including the modified stretched exponential function (MSE) (see Appendix A 2), and the complex power-law function (CPL) (see Appendix A 3) [42–46]. In cases where multiple competing processes occur on similar timescales, a multicomponent fit may be used to deduce the dominant decay routes (see Appendix A 1). In both samples, the multicomponent fit indicates that in the high-temperature regime, thermal processes dominate and the decay is satisfactorily fit by two simple exponential components. By plotting the logarithm of half-lifetime versus reciprocal temperature (Fig. 10), the

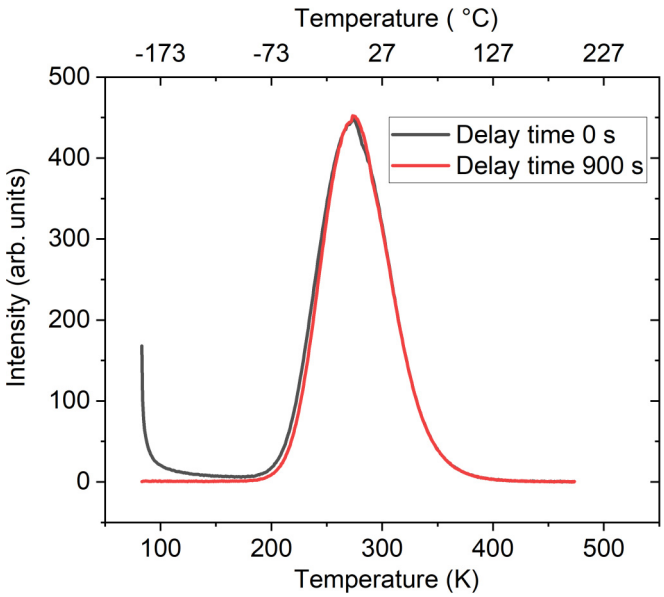

FIG. 8. By delaying the start of the TL temperature ramp, defect centers which relax via phosphorescence can be eliminated from the subsequent TL glow curve. Here, sample C{111} was excited using a 224 nm laser at 83 K and then heated at 100 K min^{-1} after the indicated post-laser delay.

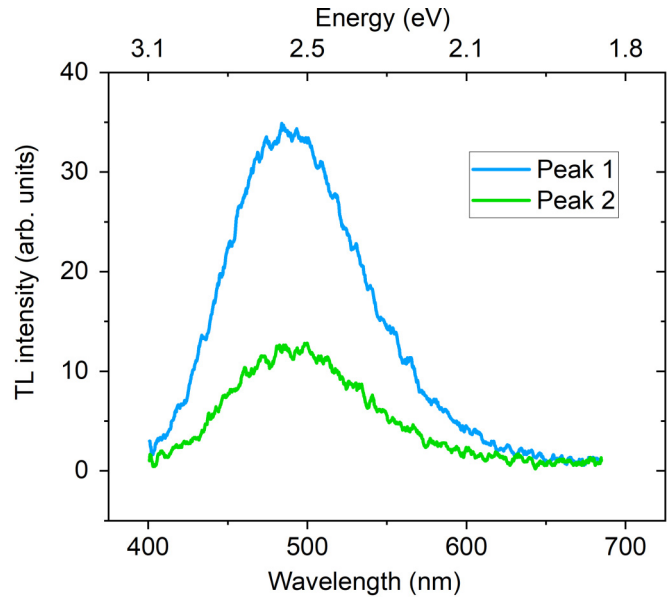

FIG. 9. TL spectra at the peak temperature of "Peak 1" (269 K) and "Peak 2" (298 K) (after thermal cleaning) in sample C{111}.

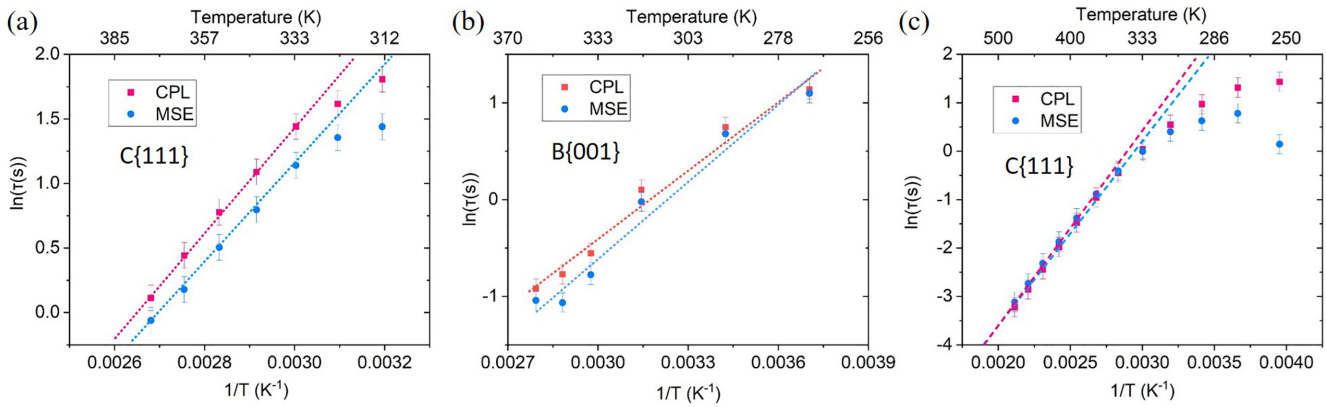

FIG. 10. The logarithm of half-lifetime (fit by the MSE function and the CPL function, respectively) vs reciprocal temperature. The dashed lines are the results of the fitting to an Arrhenius function. (a) Integrated area of 2802 cm^{-1} absorption peak (B_S^0) decay in C{111}; (b) integrated intensity of N_S^0 central EPR peak recovery in B{001}; (c) phosphorescence decay in C{111} after 224 nm excitation.

activation energy of [B_S^0] decay (333–373 K), [N_S^0] decay (210–250 K)/recovery (270–347 K), and phosphorescence decay (273–473 K) can be determined (using the Arrhenius equation) and are listed in Tables II and III.

The activation energies determined for [B_S^0] decay in both samples are similar with an average value only slightly smaller than the ionization energy of the substitutional boron acceptor (0.37 eV [3]).

The activation energies of the [N_S^0] recovery in B{001} determined by different methods are consistent and approximately 0.2 eV. In sample C{111}, measurements could not be made over a sufficiently wide temperature window, due to weak N_S^0 EPR signal strength and small optically induced changes in this signal, to accurately determine the activation energy for [N_S^0] decay.

At sufficiently high temperatures, the activation energies for phosphorescence decays as determined by different fitting methods are in reasonable agreement. The average activation energy determined from sample C{111} is only slightly below that of the boron acceptor, while those from sample B{001} are significantly below, suggesting that there is an important contribution from another trap with a significantly lower activation energy.

In the TL experiment, the depth of two traps were determined by the initial rise method and are listed in Tables II and III. Accurate trap energies are difficult to determine for closely overlapping peaks, but the involvement of a trap with lower energy than the boron acceptor is suggested.

B. Charge transfer

In sample B{001} where [N_S] > [B_S], band-gap 224 nm excitation decreases [N_S], and when the illumination is removed, the concentration recovers back to the value measured prior to band-gap illumination [Fig. 3(b)]. If the substitutional nitrogen defect can only exist in a neutral charge state and a positive charge state, the concentration of the neutral substitutional nitrogen is always expected to be increased (or not change) upon band-gap UV excitation in a sample containing only comparable quantities of substitutional nitrogen and boron defects (i.e., band-gap excitation creating free electrons and holes will tend to neutralize donors and acceptors). However, the fact that this is not the case reveals that upon band-gap UV illumination, another charge state of the substitutional nitrogen defect is produced. Therefore, it is proposed that the substitutional nitrogen defect can trap an electron to produce N_S^-, and this "acceptor level" is only ∼0.2 eV below the conduction-band minimum (Table II). When N_S^- is thermally ionized, the released electron can be trapped by N_S^+ and thus the concentration of N_S^0 can be increased. When boron acceptors are present after band-gap UV illumination is removed, DAP recombination will act to reduce the concentration of the neutral and negatively charged substitutional nitrogen defects.

Several conclusions about the charge-transfer processes can be drawn:

(i) For the substitutional nitrogen defect, three charge states have to be considered: negative, neutral, and positive. The

TABLE II. Activation energies of phosphorescence decay, TL glow peaks, B_S^0 decay, and N_S^0 recovery after band-gap optical excitation in sample B{001} where [N_S] > [B_S].

	Multiple components			
E_A (eV)	Component 1	Component 2	MSE	CPL
Phosphorescence	0.21(5)	0.23(5)	0.30(5)	0.25(5)
Thermoluminescence	0.30(5)	0.33(5)		
B_S^0 decay	0.32(5)	0.34(5)	0.32(5)	0.37(5)
N_S^0 recovery	0.18(5)	0.21(5)	0.22(5)	0.21(5)

TABLE III. Activation energies of phosphorescence decay, TL glow peaks, B_S^0 decay, and N_S^0 decay after band-gap optical excitation in sample C{111} where $[B_S] > [N_S]$.

	Multiple components			
E_A (eV)	Component 1	Component 2	MSE	CPL
Phosphorescence	0.31(5)	0.33(5)	0.34(5)	0.35(5)
Thermoluminescence	0.34(5)	0.37(5)		
B_S^0 decay	0.34(5)	0.41(5)	0.32(5)	0.35(5)
N_S^0 decay	>0.18	>0.26	>0.18	>0.19

total concentration of substitutional nitrogen is given by

$$[N_T] = [N_S^-] + [N_S^0] + [N_S^+]. \quad (1)$$

(ii) For the substitutional boron defect, only the neutral and negatively charged states should be considered. The total concentration of substitutional boron is given by

$$[B_T] = [B_S^-] + [B_S^0]. \quad (2)$$

(iii) Equilibrium charge balance is maintained such that after free carriers are trapped,

$$[N_S^-] + [B_S^-] = [N_S^+]. \quad (3)$$

(iv) Near- or above-band-gap excitation generates pairs of free carriers or excitons. Free-carrier recombination can happen through multiple relaxation channels including trapping. In diamond containing only substitutional nitrogen and boron impurities in low concentration, both tunneling between traps and thermal excitation of carriers from traps must be considered.

(v) Near- or above-band-gap excitation will increase the concentration of neutral substitutional boron acceptors:

$$B_S^- + h_{VB}^+ \rightarrow B_S^0. \quad (4)$$

(vi) Near- or above-band-gap excitation can either increase $[N_S^0]$,

$$N_S^+ + e_{CB}^- \rightarrow N_S^0, \quad (5)$$

or decrease $[N_S^0]$,

$$N_S^0 + e_{CB}^- \rightarrow N_S^-. \quad (6)$$

Optical excitation with sufficient (below-band-gap) energy to ionize N_S^0 can also decrease the concentration of N_S^0:

$$2N_S^0 \xrightarrow{\hbar\omega} N_S^+ + N_S^-. \quad (7)$$

(vii) N_S^0 is a deep donor, and at the temperatures studied the probability of thermal ionization is negligible. However, N_S^- is readily thermally ionized over a temperature range which overlaps with that for thermal ionization of B_S^0.

C. "Blue-green" phosphorescence mechanism

The characteristic narrow lines associated with DAP emission from close pairs (separation of order or less than the sum of the donor and acceptor radii) that accompany the broad emission from distant pairs in other materials (e.g., GaP, 3C-SiC) with shallow, delocalized donors and acceptors are not observed in this work [47,48]. Given the compact donor and acceptor wave functions in diamond, there are very few neighbors that should even be considered as "close pairs." Although Dischler *et al.* tentatively interpreted that CL emission features are arising from close DAP in CVD diamond, this assertion has not been confirmed and the intensities were not in accord with theory [49].

To identify the "blue-green" luminescence center, Wantanable *et al.* suggested B_S^0 as the acceptor, and nitrogen in different forms could act as the donor [6]. The $N_S^0 \cdots B_S^0$ DAP recombination was asserted by Ščajev *et al.* since N_S and B_S are the most abundant defects/impurities in near-colorless HPHT diamond [50], and this assignment had previously been erroneously ruled out or overlooked [9]. The "blue-green" emission observed in all the samples studied in this work would also be expected in CVD and natural diamonds codoped with N_S and B_S.

When modeling the donor-acceptor pair recombination process, the nitrogen donor changes the charge state from N_S^0 to N_S^+, and there is a large configuration change that should not be ignored. (N_S^0 has C_{3v} symmetry with one N-C bond 25% longer than the diamond C-C bond, and the other three smaller, whereas N_S^+ has T_d symmetry with all N-C bonds approximately equal to the diamond C-C bond length [51].) However, when the boron acceptor changes the charge state from B_S^0 to B_S^-, there is little configurational change (in both charge states the defect has T_d symmetry; any symmetry-lowering distortion is negligible [52]). It can be seen from a 1D configuration coordinate diagram (Fig. 11) that for a $N_S^0 \cdots B_S^0$ pair to emit a photon, a substantial amount of energy must be lost to the emission of a significant number of phonons. Figure 11 has been drawn assuming a typical N_S^0 phonon energy of 1130 cm^{-1} ($\hbar\Omega_0 = 141$ meV) [32] and a B_S^0 phonon energy of 427 cm^{-1} ($\hbar\Omega_0 = 53$ meV) [53] and that the energy lost to phonons in the configuration change associated with emission is approximately 1.2 eV. Taking this into account, the energy of the DAP recombination transition energy should be given by

$$\hbar\omega = E_g - (E_D + E_A) + \Delta E_C - \Delta_{FC}^g, \quad (8)$$

where ΔE_C is the Coulombic correction term and Δ_{FC}^g is the Frank-Condon shift. Δ_{FC}^g can be expressed as SE_{ph}, where the Huang-Rhys factor S essentially qualifies the average number of phonons emitted per transition (in this case, approximately 23) and E_{ph} is the average phonon energy [54]. Such strong electron-phonon coupling is unsurprising for such a deep localized donor. This is consistent with the description of

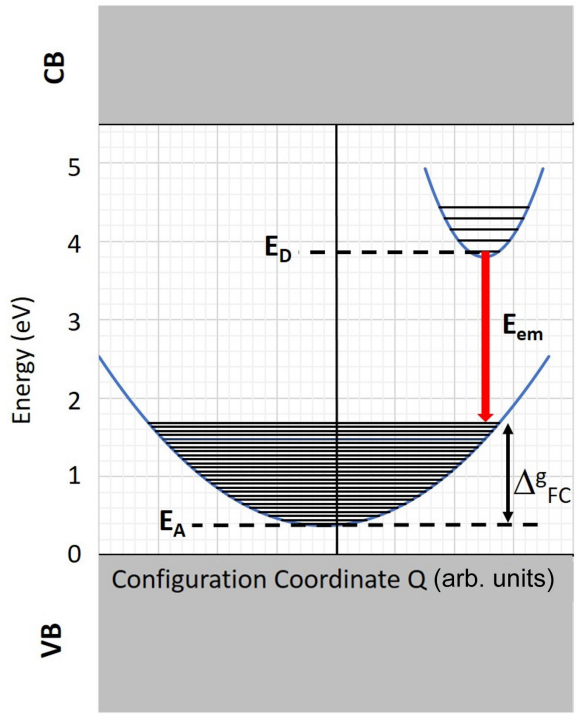

FIG. 11. The configuration diagram for the energy levels of boron-nitrogen pair recombination at 0 K. The electronic state of substitutional nitrogen is 1.7 eV below the conduction band, and the ionization energy of boron is 0.37 eV.

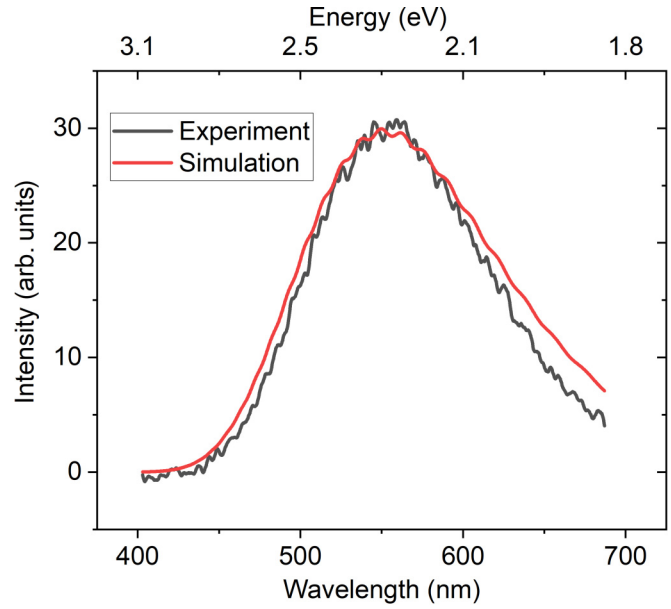

FIG. 12. Phosphorescence spectrum at 173 K in C{111} (black line), and simulated spectrum with parameters $E_g = 5.47$ eV, $E_D = 1.7$ eV (N_S^0), $E_A = 0.37$ eV (B_S^0), $E_{ph} = 53$ meV, $S = 22.7$: ΔE_C is assumed zero (see text).

$N\cdots B$ pair recombination emission hypothesized by Ščajev *et al.* [50].

The Frank-Condon shift $\Delta^g_{FC} = 1.2$ eV would result in a distant $N_S^0\cdots B_S^0$ pair emission energy of approximately 2.25 eV, consistent with the observations reported here and elsewhere. Given the large configuration change, such a large Frank-Condon shift appears reasonable; indeed, in molecules the shifts can be as large as several eV [55]. We note that the barrier to the reorientation of the N_S^0 C_{3v} axis has been estimated as approximately 0.8 eV [56], and the energy of the N_S^0 donor level is deeper than the value predicted for a hydrogenic donor (∼0.4 eV) by ∼1.3 eV. Both values are large compared to shifts observed in other materials, and they demonstrate the large configurational change associated with N_S^0. Further theoretical calculations of the Frank-Condon shift for emission from a $N_S^0\cdots B_S^0$ pair would be very valuable.

To describe the vibrational broadening of the $N_S^0\cdots B_S^0$ pair emission, it is necessary to sum all possible transitions between the accessible vibrational levels of the N_S^0 donor and all those of the associated B_S^0 acceptor. Assuming a typical N_S^0 phonon energy of $\hbar\Omega_0 = 141$ meV, then at room temperature (k_BT ∼26 meV) only the ground vibrational state of the N_S^0 donor will be occupied, and thus using the 1D model it is only necessary to sum over all the vibrational levels of B_S^0 using the equation

$$I(E) = \sum_n e^{-S}\,\frac{S^n}{n!}\,g_\Gamma\,(E_{ZPL} - nE_{ph} - E), \qquad (9)$$

where $n = 1, 2, 3\ldots$ are the phonon replicas, E_{ph} is the average phonon energy, and g_Γ is a Gaussian function with a parameter Γ defining the width of the Gaussian peak [57]. Strictly speaking, this equation is derived assuming that the vibrational energies of the ground and excited state are equal, but a similar result is obtained if they are not [54,58]. For defects with large electron-phonon coupling ($S \gg 1$), resolved phonon replicas are not observed, and contributions from individual phonon modes cannot be identified. Furthermore, the luminescence intensity from the zero-phonon line of each different $N_S^0\cdots B_S^0$ pair is practically zero. Figure 12 shows a simulation of the distant (small Coulomb shift) $N_S^0\cdots B_S^0$ pair emission in the limit of strong electron-phonon coupling ($S \sim 23$), using Eq. (9). The agreement between simple theory and experiment is reassuring. The broadening of the emission lines from the very few close pairs means that they are undetectable, and the overlapping contributions from differently separated distant pairs (with different relaxation times) provide a natural explanation of the complex nonexponential decay.

Before illumination, we expect a significant latent population of N_S^+ and B_S^-. In the same sample, significant populations of isolated N_S^0, N_S^-, and B_S^0 can be produced by near- or above-band-gap excitation. At low temperatures, there is essentially no thermal excitation of carriers to the conduction or valence band, and hence these defects are isolated, with only relatively close defects able to exchange charge via tunneling. Sufficiently close $N_S^0\cdots B_S^0$ pairs can emit light:

$$N_S^0\cdots B_S^0 \rightarrow N_S^+\cdots B_S^- + \hbar\omega \qquad (10)$$

but only a very few have sufficiently close donors and acceptors to be reset into the "ready to emit" $N_S^0\cdots B_S^0$ state by tunneling. Thus, low temperature phosphorescence would be dominated by long-lived relatively distant $N_S^0\cdots B_S^0$ pairs. Although their emission probability is typically low (long lifetime), there is a large population of them, and no other processes are operating to modify the charge states of these

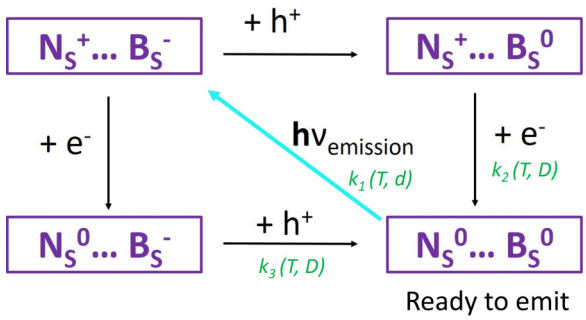

FIG. 13. Schematic of the reset of $N_S^0 \cdots B_S^0$ luminescence center. The rate constants of different charge-transfer processes are labeled as $k_1(T, d)$, $k_2(T, D)$, $k_3(T, D)$ and will be discussed below.

pairs' constituents. As the temperature is increased, the probability of thermal ionization of N_S^- and B_S^0 increases rapidly. Carriers are released into the conduction and valence bands, and defects are "connected" by free carriers in these bands. Close $N_S^0 \cdots B_S^0$ pairs can emit, and may reemit via the subsequent capture of both an electron and a hole. It is likely that distant $N_S^0 \cdots B_S^0$ pairs will have one or both constituents ionized before they emit. Thus at high temperature, close pairs with higher energies will dominate the emission (Fig. 13).

The energy at which a $N_S^0 \cdots B_S^0$ pair emits depends on the separation of the nitrogen donor and the boron acceptor, with the Coulomb correction term increasing as the separation between the donor and acceptor decreases. Statistically, there will be very few close pairs. The emission probability is higher for close pairs, thus the lifetime is shorter.

Once a neutral donor-acceptor pair has emitted, both electron and hole capture (regardless of the order) are required to enable the pair to emit again, as shown in Fig. 13. By resetting the charge states of the donor and the acceptor, it is possible for each luminescence center to emit multiple times.

At low temperatures when there is no thermal activation of carriers, the emission will be dominated by distant pairs, and the majority of pairs will emit only once. Thus the peak emission will be at slightly lower energies (2.25 eV). As the temperature increases, the probability of thermal ionization increases and closer pairs can be reset by charge capture and emit multiple times. Furthermore, the long-lived distant pairs will be increasingly ionized before they can emit. Thus the emission peak will shift to higher energies (2.5 eV) as the temperature is increased. The magnitude of the shift observed is 0.25 eV, which is consistent with the Coulomb correction term.

We can write a rate equation for the loss of $N_S^0 \cdots B_S^0$ (Fig. 13) via light emission as below:

$$-\frac{d\left[N_S^0 \cdots B_S^0\right]}{dt} = k_1\left[N_S^+ \cdots B_S^-\right] - k_2\left[N_S^+ \cdots B_S^0\right][e^-] - k_3\left[N_S^0 \cdots B_S^-\right][h^+], \quad (11)$$

where $k_1(T, d)$, $k_2(T, D)$, $k_3(T, D)$ are the rate constants of different charge-transfer processes labeled in Fig. 13. This rate equation cannot be solved since $k_1(T, d)$ depends on both temperature (i.e., whether the rate is dominated by thermal or tunneling processes, or mixed) and the distance d between donor and acceptor. Both $k_2(T, D)$ and $k_3(T, D)$ depend both on the temperature-dependent mechanisms of the charge-transfer processes, and the distance D between the trap and subsequent luminescence center (DAP). Within each sample, there is a very broad distribution of distances between either the donor and acceptor, or the isolated trap and the luminescence center (DAP). In addition, the decay rate decreases during the phosphorescence decay instead of remaining constant (see Appendix A 2).

There is expected to only be a small configuration change between N_S^0 and N_S^-. The emission from a $N_S^- \cdots B_S^0$ pair is expected to be in the UV range: if the Franck-Condon shift for this emission was ∼1.2−1.7 eV, we estimate the DAP peak from $N_S^- \cdots B_S^0$ pairs to be at ∼3.2−3.7 eV. The CL emission band at 390 nm (3.2 eV) observed in sample B at 80 K (Fig. 5) may originate from $N_S^- \cdots B_S^0$ pair recombination.

V. CONCLUSIONS

Since the "blue-green" phosphorescence spectrum, lifetime, and intensity vary between growth sectors in near-colorless HPHT diamonds, it is important to study individual growth sectors in order to interpret the emission mechanism and defects involved.

The data presented here confirm that the substitutional nitrogen defect in diamond has an acceptor state approximately 0.2 eV below the bottom of the conduction band. This is shallower than predicted by theory [34], but interestingly such a low activation energy has been reported in previous studies [11,20,22,24] on natural and HPHT grown diamonds.

It is shown that the broad "blue-green" luminescence and phosphorescence band can be fully explained by emission from $N_S^0 \cdots B_S^0$ donor-acceptor pairs, once the configurational change between charge states is considered. At sufficiently high temperatures, $N_S^0 \cdots B_S^0$ luminescence pairs can be reset multiple times by capture of electrons and holes thermally ionized from N_S^- and B_S^0, respectively. The "blue-green" phosphorescence mechanism switches at low temperatures, where the probability of thermal ionization is negligible, to one where charge-carrier tunneling dominates. The shift of the phosphorescence peak energy with increasing temperature and delay after the excitation is removed is consistent with the properties of the model proposed.

The presence of both relatively shallow donors and acceptors is essential in order to reset the nitrogen-boron donor acceptor pairs into the ready-to-emit state ($N_S^0 \cdots B_S^0$) multiple times. This resetting of emitters facilitates bright and long-lived phosphorescence from a low concentration of relatively close donor-acceptor pairs. It must be remembered that in an insulating material like diamond, the calculated position of the Fermi level does not necessarily predict the correct charge state of a defect, and the defect charge state is strongly influenced by the proximity of a particular defect to a donor (or acceptor). After at or above-band-gap excitation of near-colorless diamond doped with relatively low concentrations of substitutional nitrogen and boron defects, at temperatures where the probability of thermal ionization is low, there can be significant populations of isolated N_S^0, B_S^0, and N_S^- defects that persist almost indefinitely.

This work predicts that UV luminescence should arise from $N_S^- \cdots B_S^0$ donor acceptor pairs: a possible candidate emis-

sion was observed in low-temperature cathodoluminescence in this study, but further study is required. The "blue-green" luminescence and phosphorescence should be observed in diamond grown by chemical vapor deposition and codoped with nitrogen and boron. In this work, the concentration of $N_S^0 \cdots B_S^0$ pairs that are sufficiently close to give rise to optical emission has not been identified. It is usually assumed that the distribution of donors and acceptors will be random, but it is not possible to rule out preferential incorporation of close pairs, or the production of pairs upon annealing and defect migration. Further work is required to address this question.

ACKNOWLEDGMENTS

J.Z. thanks De Beers Ignite for providing funding. We thank the late Dr. Tom Anthony of the General Electric Research & Development Centre for provision of samples used in this work, and Prof. Rachel Oliver and Dr. Gunnar Kusch for their assistance with cathodoluminescence measurement at Cambridge Centre for Gallium Nitride. B.L.G. gratefully acknowledges the Royal Academy of Engineering for a Research Fellowship. B.L.G. and M.E.N. acknowledge funding from EPSRC via Grant No. EP/V056778/1.

APPENDIX: DECAY/RECOVERY CURVE-FITTING METHODS

1. Multiple component fitting

The athermal tunneling process does not involve the conduction band or the valence band but occurs between traps (donors or acceptors) and nearby luminescence centers with aligned energy levels in the band gap [44,59]. The probability of tunneling is determined by the overlap of the trap/luminescence center wave functions. Generally speaking, a high concentration of related defects enables the formation of close trap-center pairs for tunneling [44]. The tunneling process is also achievable between far distance trap and luminescence center by a chainlike path which consists of several traps delivering carriers to the luminescence center when the concentration of traps is high [44]. Only considering pairs containing one variety of trap and luminescence center separated by a distance r (ignoring the chainlike path tunneling), the phosphorescence intensity is given by

$$I(t) = \frac{I_0}{(1 + t/\tau)}, \tag{A1}$$

where the lifetime τ depends on the intensity of excitation [60].

For a thermally activated process, electrons or holes are trapped at localized energy levels during optical excitation. After excitation, those trapped charge carriers can be thermally released into the conduction band or the valence band and then retrapped at an isolated trap or radiatively recombine at a center, at which light may be subsequently emitted. The relative number of traps and luminescence centers determines whether retrapping or the radiative recombination process dominates [17,44]. When the concentration of luminescence centers is much higher than that of traps, recombination dominates, and the phosphorescence process follows first-order kinetics (only one variety of luminescence center and one variety of trap are involved). The intensity of phosphorescence is described as

$$I(t) = I_0 \exp\left(-\frac{t}{\tau}\right), \tag{A2}$$

where I_0 is the initial intensity; at very high temperature, I_0 decreases. t is a delay time, τ is the lifetime of traps,

$$\frac{1}{\tau} = \frac{1}{s} \exp\left(-\frac{E_{\text{trap}}}{k_B T}\right), \tag{A3}$$

where s is a constant, which may, however, vary slowly with temperature, E_{trap} is the depth of the trap, and T is the temperature. Therefore, for a constant T, the decay follows a simple exponential decay [17,44]. When traps are more abundant, both retrapping and recombination are considered; if we assume the initial number of trapped carriers and the initial number of luminescence centers available for recombination are both equal to n_0, the phosphorescence process follows second-order kinetics. The intensity of phosphorescence is described as

$$I(t) = \frac{I_0}{(n_0 \alpha t + 1)^2}. \tag{A4}$$

The constant α describes the relative possibilities of the retrapping and the recombination processes. The phosphorescence decay follows a power-law decay with the power of two, namely a hyperbolic decay [17].

Multiple varieties of traps and luminescence centers may participate in the thermal and tunneling processes. The phosphorescence decay, therefore, could be considered as the combination of multiple decay components. Accordingly, the intensity of phosphorescence is described by

$$I(t) = \sum_m \frac{I_0}{(1 + t/\tau)} + \sum_n I_0 \exp\left(-\frac{t}{\tau}\right) + \sum_p \frac{I_0}{(n_0 \alpha t + 1)^2}, \tag{A5}$$

where m, n, and p are integers $\geqslant 0$, representing the number of components belonging to $1/t$ power-law decay, simple exponential decay, and hyperbolic decay in phosphorescence, respectively.

2. Stretched exponential function

The stretched exponential function, as a sum of exponential decay, is robust to describe complex thermally activated luminescence decay considering the diversity of impurities and charge-transfer paths, as well as the random distribution traps [42,61]. During phosphorescence decay, the number of available luminescence centers is reduced, thereby free carriers in the conduction band or the valence band must travel for a longer distance before activating recombination at luminescence centers, leading to a decrease in the phosphorescence decay rate. The stretched exponential function described such a luminescence decay without a constant decay rate with the assumptions of at least one trapping state and one variety of luminescence center involved, the direct band-to-band recombination is negligible, and retrapping is considered [43]. The intensity of phosphorescence decay described by a stretched

exponential function, which is also called the Kohlrausch function, is written as

$$I(t) = I_0 \exp\left[-\left(\frac{t}{\tau_0}\right)^{\beta}\right], \tag{A6}$$

where I_0 is the initial intensity, t is a delay time, τ_0 is a parameter with the dimensions of time, and β is a dispersion exponent with a range of $0 < \beta < 1$ [42,43]. The time-dependent rate coefficient $k(t)$ is

$$k(t) = \frac{\beta}{\tau_0}\left(\frac{t}{\tau_0}\right)^{\beta-1}. \tag{A7}$$

When $k(t)$ is constant, the decay is an exponential decay. When $k(t)$ increases or decreases with time, the decay described is a superexponential decay or a subexponential decay, respectively [42].

The infinite initial decay rate of the stretched exponential function is obviously not in accordance with the understanding of phosphorescence decay. To solve the problem of fitting the first several experimental data points of the decay curve, a modified stretched exponential (MSE) function is created to enable the selection of the origin of times t_0 comparing with τ_0. A parameter α is defined as t_0/τ_0. Hence, the modified exponential function for phosphorescence decay is

$$I(t) = \exp\left[\alpha^{\beta} - \left(\alpha + \frac{t}{\tau_0}\right)^{\beta}\right]. \tag{A8}$$

The time-dependent rate coefficient is

$$k(t) = \frac{\beta}{\tau_0}\left(\alpha + \frac{t}{\tau_0}\right)^{\beta-1}. \tag{A9}$$

The lifetime of phosphorescence is given by

$$\tau = \tau_0 \frac{\tau^{1-\beta}}{\beta}. \tag{A10}$$

In summary, a better approach of experimental fits for phosphorescence decay of complex thermal processes is provided by a modified stretched exponential function [44]. While the modified stretched exponential function is not a complete model of phosphorescence decay, it does achieve better accuracy in calculating the activation energy.

3. Complex power-law function

A complex power-law function (compressed hyperbola) was devised by Becquerel to provide a more general solution for phosphorescence decay fitting as a supplement to the exponential function and to accommodate more possible factors, such as the distribution of traps with different depth and the interaction of different luminescence centers. The equation is written as

$$I(t) = \frac{I_0}{(1+at)^p}, \tag{A11}$$

where I_0 is the initial intensity, a is a constant, and p is the power between 1 and 2 [45,46].

[1] R. G. Farrer, Solid State Commun. **7**, 685 (1969).
[2] I. Stenger, M.-A. Pinault-Thaury, T. Kociniewski, A. Lusson, E. Chikoidze, F. Jomard, Y. Dumont, J. Chevallier, and J. Barjon, J. Appl. Phys. **114**, 073711 (2013).
[3] A. T. Collins, Philos. Trans. R. Soc. London A **342**, 233 (1993).
[4] V. Sonin, A. Tomilenko, E. Zhimulev, T. Bul'ak, A. Chepurov, Y. Babich, A. Logvinova, T. Timina, and A. Chepurov, Sci. Rep. **12**, 1246 (2022).
[5] Type II: diamond contains very low level of nitrogen impurities (<1 ppm).
[6] K. Watanabe, S. C. Lawson, J. Isoya, H. Kanda, and Y. Sato, Diam. Relat. Mater. **6**, 99 (1997).
[7] S. Eaton-Magaña and C. M. Breeding, Gems Gemol. **52**, 2 (2016).
[8] U. F. S. D'Haenens-Johansson, A. Katrusha, K. S. Moe, P. Johnson, and W. Wang, Gems Gemol. **51**, 260 (2015).
[9] S. Eaton-Magaña and R. Lu, Diam. Relat. Mater. **20**, 983 (2011).
[10] S. Eaton-Magaña, J. E. Post, P. J. Heaney, J. Freitas, P. Klein, R. Walters, and J. E. Butler, Geology **36**, 83 (2008).
[11] P. S. Walsh, E. C. Lightowlers, and A. T. Collins, J. Lumin. **4**, 369 (1971).
[12] Z. Song, T. Lu, S. Tang, J. Ke, J. Su, B. Gao, N. Hu, J. Zhang, J. Zhou, L. Bi *et al.*, J. Gemmol. **35**, 140 (2016).
[13] V. Chandrasekharan, *Proceedings of the Indian Academy of Sciences-Section A* (Springer, India, 1946), Vol. 24, pp. 182–186.
[14] V. Chandrasekharan, *Proceedings of the Indian Academy of Sciences-Section A* (Springer, India, 1946), Vol. 24, p. 187.
[15] J. B. Krumme and W. J. Leivo, *Proceedings of the Oklahoma Academy of Science* (The Oklahoma Academy of Science, 1964), Vol. 44, pp. 105–114.
[16] L. Su, C. Zhao, Q. Lou, C. Niu, C. Fang, Z. Li, C. Shen, J. Zang, X. Jia, and C. Shan, Carbon **130**, 384 (2018).
[17] S. W. S. McKeever, *Thermoluminescence of Solids* (Cambridge University Press, Cambridge, 1988), Vol. 3.
[18] L. Paslovsky, J. E. Lowther, T. L. Nam, and R. J. Keddy, J. Lumin. **55**, 167 (1993).
[19] A. Petitfils, F. Wrobel, M. Benabdesselam, P. Iacconi, and J. E. Butler, Diam. Relat. Mater. **16**, 1062 (2007).
[20] A. Halperin and R. Chen, Phys. Rev. **148**, 839 (1966).
[21] J. Levinson, A. Halperin, and V. Bar, J. Lumin. **6**, 1 (1973).
[22] J. Bourgoin, B. Massarani, and R. Visocekas, Phys. Rev. B **18**, 786 (1978).
[23] C. Bull and G. F. J. Garlick, Proc. Phys. Soc. A **63**, 1283 (1950).
[24] A. Halperin and J. Nahum, J. Phys. Chem. Solids **18**, 297 (1961).
[25] T. Shao, F. Lyu, X. Guo, J. Zhang, H. Zhang, X. Hu, and A. H. Shen, Carbon **167**, 888 (2020).
[26] M. Benabdesselam, P. Iacconi, D. Briand, D. Lapraz, E. Gheeraert, and A. Deneuville, Diam. Relat. Mater. **9**, 56 (2000).
[27] J. Nahum and A. Halperin, J. Phys. Chem. Solids **24**, 823 (1963).
[28] D. Howell, A. T. Collins, L. C. Loudin, P. L. Diggle, U. F. S. D'Haenens-Johansson, K. V. Smit, A. N. Katrusha,

J. E. Butler, and F. Nestola, Diam. Relat. Mater. **96**, 207 (2019).
[29] V. D. Blank, M. S. Kuznetsov, S. A. Nosukhin, S. A. Terentiev, and V. N. Denisov, Diam. Relat. Mater. **16**, 800 (2007).
[30] G. Davies, *Properties and Growth of Diamond* (Institute of Engineering & Technology, London, 1994), Vol. 9.
[31] R. C. Burns, V. Cvetkovic, C. N. Dodge, D. J. F. Evans, M.-L. T. Rooney, P. M. Spear, and C. M. Welbourn, J. Cryst. Growth **104**, 257 (1990).
[32] M. N. R. Ashfold, J. P. Goss, B. L. Green, P. W. May, M. E. Newton, and C. V. Peaker, Chem. Rev. **120**, 5745 (2020).
[33] A. T. Collins, J. Phys.: Condens. Matter **14**, 3743 (2002).
[34] R. Jones, J. P. Goss, and P. R. Briddon, Phys. Rev. B **80**, 033205 (2009).
[35] R. Ulbricht, S. T. van der Post, J. P. Goss, P. R. Briddon, R. Jones, R. U. A. Khan, and M. Bonn, Phys. Rev. B **84**, 165202 (2011).
[36] A. T. Collins and A. W. S. Williams, J. Phys. C **4**, 1789 (1971).
[37] B. G. Breeze, Electron paramagnetic resonance studies of point defects in diamond: quantification, spin polarisation and preferential orientation, Ph.D. thesis, University of Warwick, 2016.
[38] J. Li, C. Fan, S. Chen, and G. Li, J. Gemmol. **35**, 248 (2016).
[39] S. Eaton-Magaña, Gems Gemol. **52**, 412 (2016).
[40] J. Zhao, Fluorescence, phosphorescence, thermoluminescence and charge transfer in synthetic diamond, Ph.D. thesis, University of Warwick, 2022.
[41] A. Dobrowolska, A. J. J. Bos, and P. Dorenbos, J. Phys. D **47**, 335301 (2014).
[42] M. N. Berberan-Santos, E. N. Bodunov, and B. Valeur, Chem. Phys. **315**, 171 (2005).
[43] R. Chen, J. Lumin. **102-103**, 510 (2003).
[44] A. Vedda and M. Fasoli, Radiat. Meas. **118**, 86 (2018).
[45] W. L. Medlin, Phys. Rev. **122**, 837 (1961).
[46] M. N. Berberan-Santos, E. N. Bodunov, and B. Valeur, Chem. Phys. **317**, 57 (2005).
[47] J. J. Hopfield, D. G. Thomas, and M. Gershenzon, Phys. Rev. Lett. **10**, 162 (1963).
[48] J. W. Sun, I. G. Ivanov, S. Juillaguet, and J. Camassel, Phys. Rev. B **83**, 195201 (2011).
[49] B. Dischler, W. Rothemund, C. Wild, R. Locher, H. Biebl, and P. Koidl, Phys. Rev. B **49**, 1685 (1994).
[50] P. Ščajev, L. Trinkler, B. Berzina, E. Ivakin, and K. Jarašiūnas, Diam. Relat. Mater. **36**, 35 (2013).
[51] A. Cox, M. E. Newton, and J. M. Baker, J. Phys.: Condens. Matter **6**, 551 (1994).
[52] J. P. Goss and P. R. Briddon, Phys. Rev. B **73**, 085204 (2006).
[53] V. Mortet, A. Taylor, Z. V. Živcová, D. Machon, O. Frank, P. Hubík, D. Trémouilles, and L. Kavan, Diam. Relat. Mater. **88**, 163 (2018).
[54] A. Alkauskas, M. D. McCluskey, and C. G. Van de Walle, J. Appl. Phys. **119**, 181101 (2016).
[55] A. Franceschetti and S. T. Pantelides, Phys. Rev. B **68**, 033313 (2003).
[56] C. A. J. Ammerlaan and E. A. Burgemeister, Phys. Rev. Lett. **47**, 954 (1981).
[57] K. Huang and A. Rhys, Proc. R. Soc. London A **204**, 406 (1950).
[58] A. Alkauskas, J. L. Lyons, D. Steiauf, and C. G. Van de Walle, Phys. Rev. Lett. **109**, 267401 (2012).
[59] P. Avouris and T. N. Morgan, J. Chem. Phys. **74**, 4347 (1981).
[60] P. Avouris, I. F. Chang, D. Dove, T. N. Morgan, and Y. Thefaine, J. Electron. Mater. **10**, 887 (1981).
[61] J. C. Phillips, Rep. Prog. Phys. **59**, 1133 (1996).